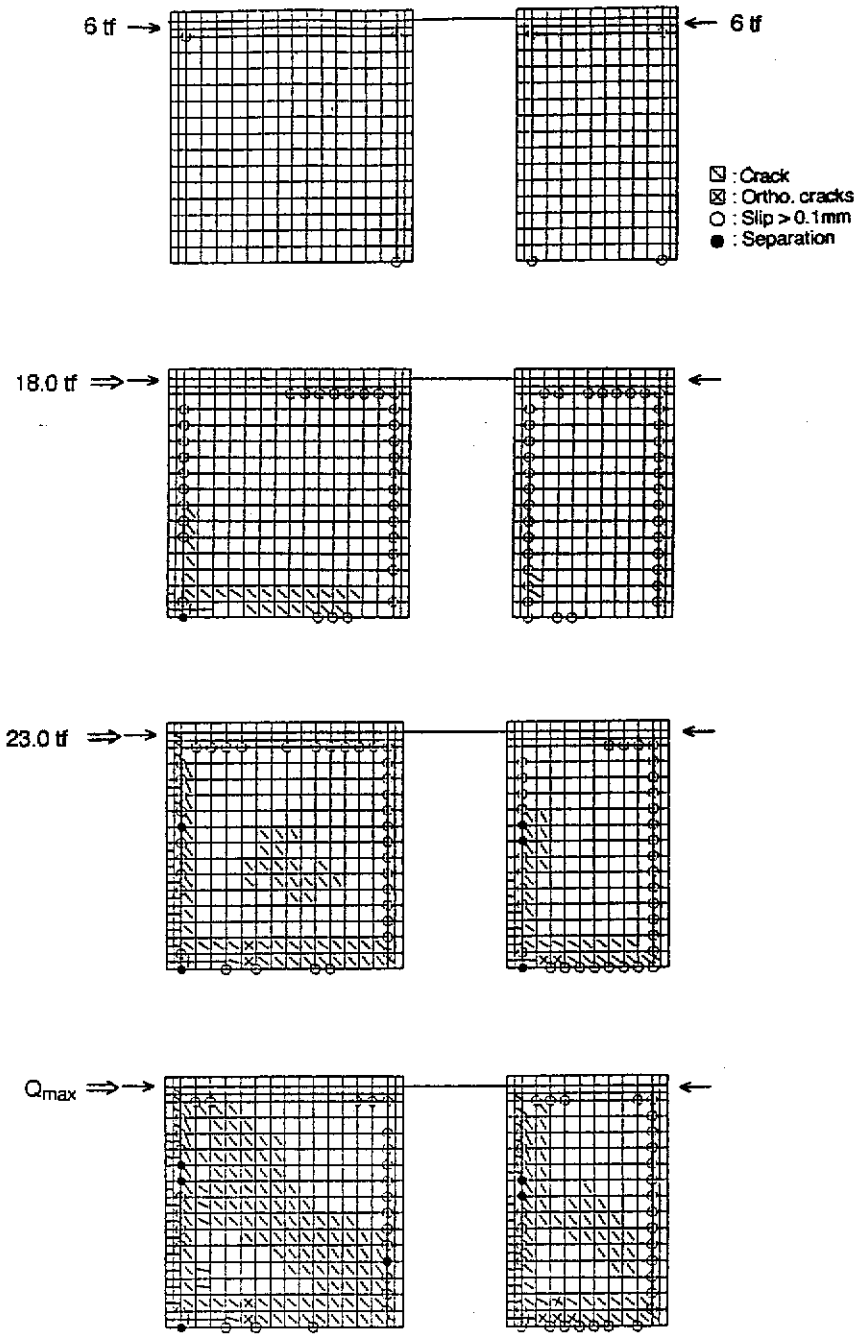

Fig. 7.2.11 Crack development in Case 7: W-W, positive loading, vertical load 25tf, pretension force of 6 t

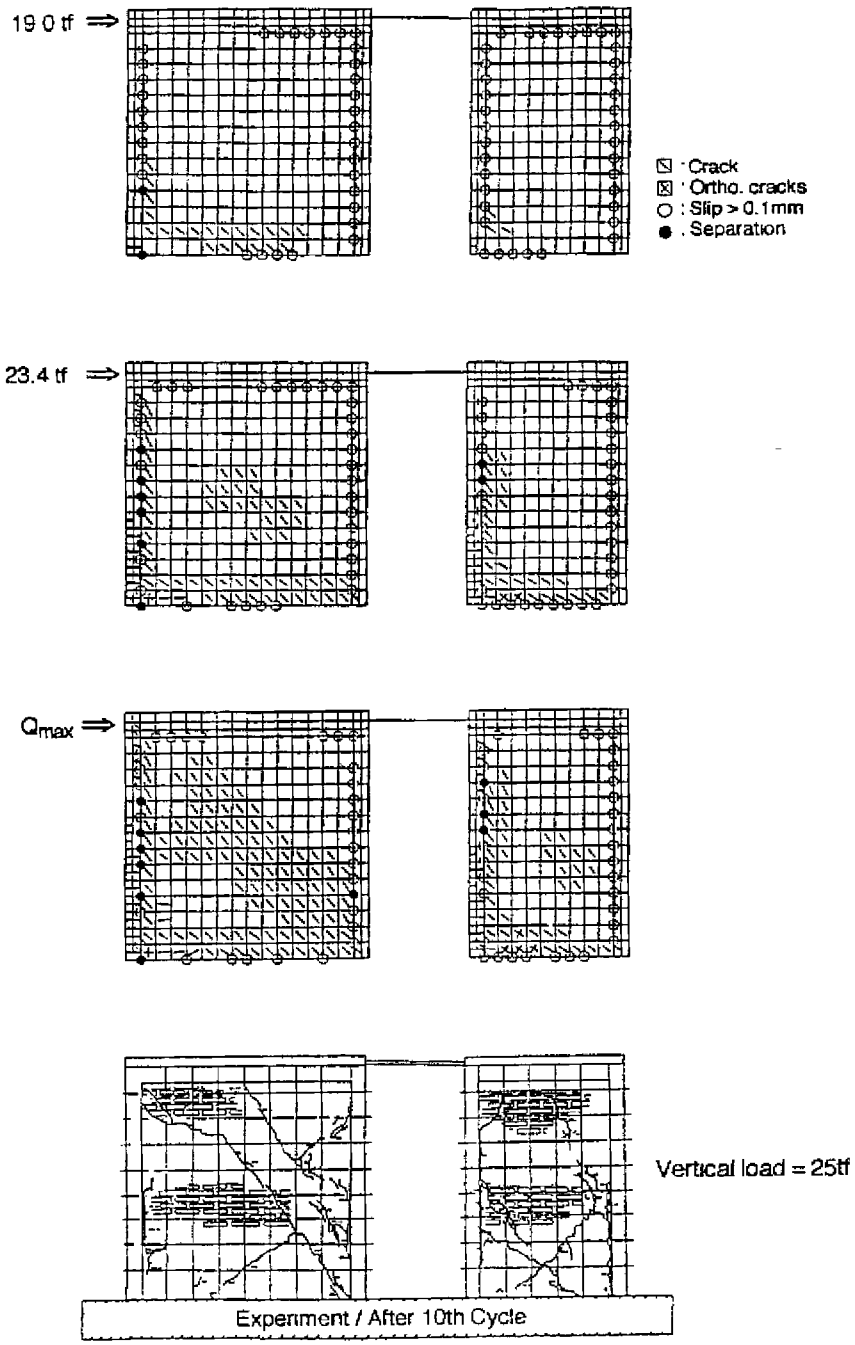

Fig. 7.2.12 Crack development in Case 8: W-W, positive loading, vertical load 30tf

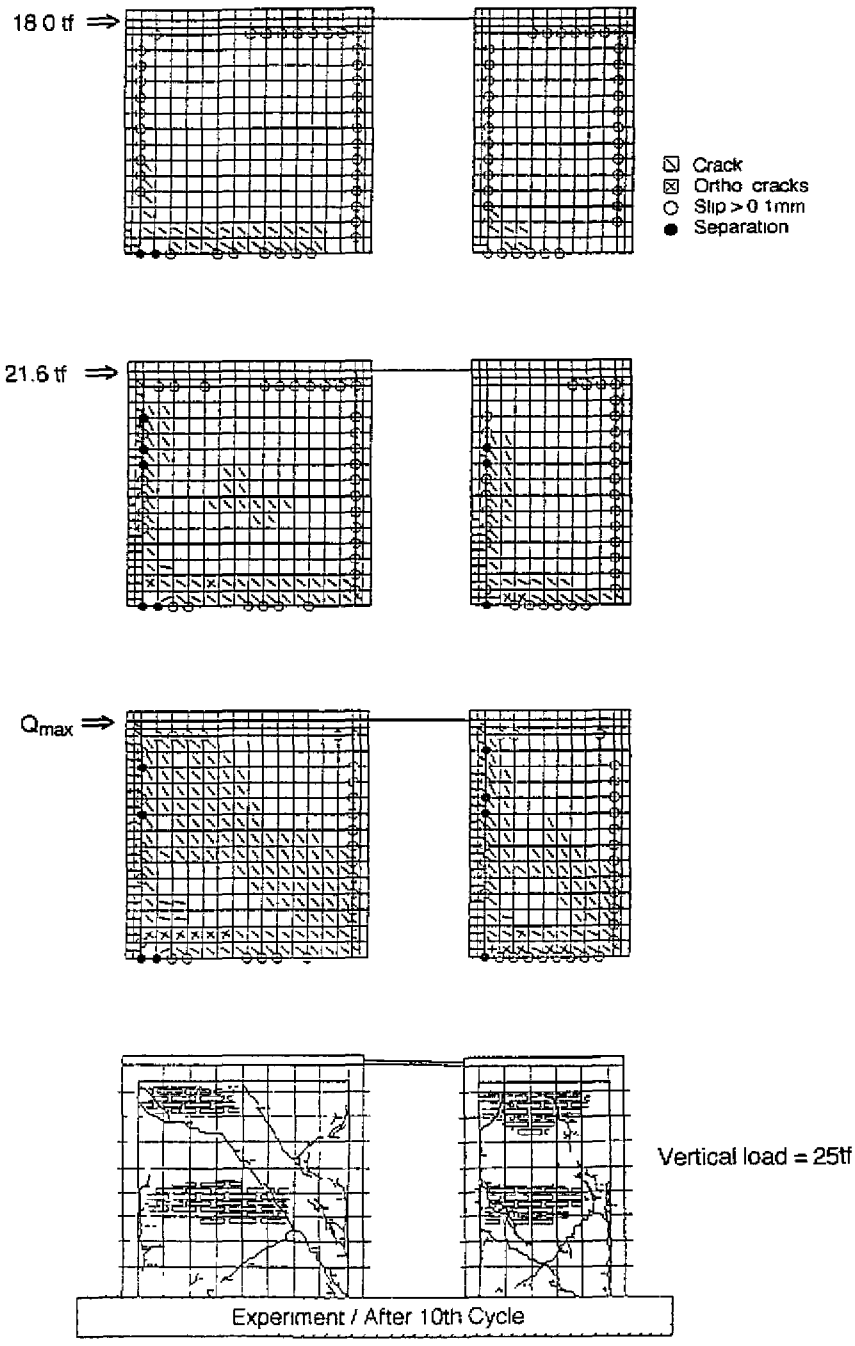

Fig. 7.2.13 Crack development in Case 9: W-W, positive loading, vertical load 20tf

7.3 Case 10 and 11; Specimen WWW

In Fig. 7.3.1, horizontal displacement relations calculated in Cases 10 and 11 are compared with the corresponding hysteretic curve obtained in the experiment. Ultimate shear strengths and drift angles caused at ultimate states are listed on Table 7.3 in comparison with test results. It is observed from the figure and table that elastic rigidities and ultimate shear strengths are in general in good agreement with test results, but there is a big difference in drift angles at ultimate strengths between calculated values and test results.

Table 7.3 Ultimate shear strengths and corresponding drift angles in Cases 10 and 11

Case	Ultimate Shear Strength			Drift Angle at Ultimate Strength	
	Test (tf)	Cal. (tf)	Test/Cal.	Test (10^{-3})	Cal. (10^{-3})
10	25.9	27.3	0.95	1.62	1.24
11	28.5	27.0	1.06	3.08	1.54

Computed deformation patterns at a horizontal load of 18tf are shown in Figs 7.3.2 and 7.3.3 in comparison with test results. Crack development is shown in Figs 7.3.4 and 7.3.5, where crack patterns for a horizontal load corresponding to the ultimate shear strength are compared with those recorded in the experiments.

Calculated deformation patterns and calculated crack patterns in brick walls are in good agreement with test results. However, slip or separation along boundary surfaces between columns and brick walls, which were not observed in the experiment, were obtained in the analyses.

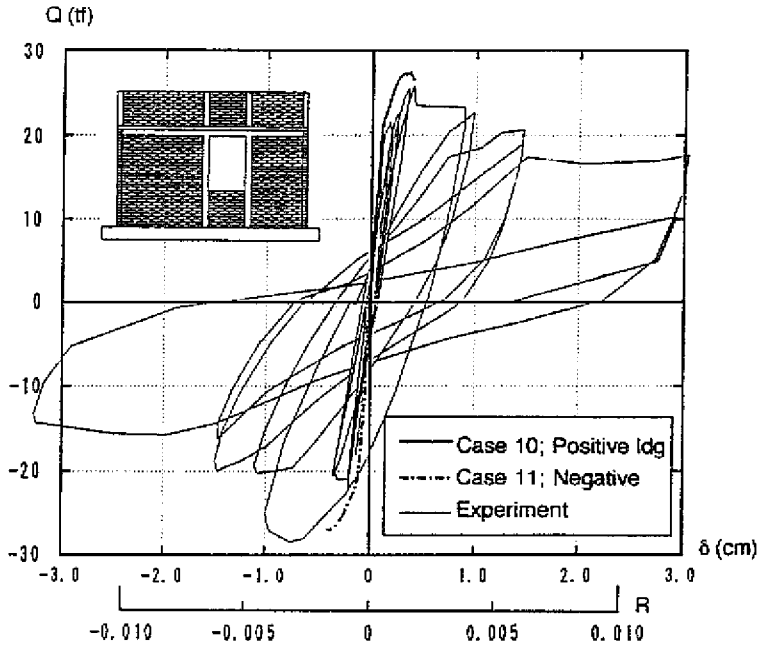

Fig. 7.3.1 Load (Q)-displacement (δ) relationships calculated in Case 10 and Case 11

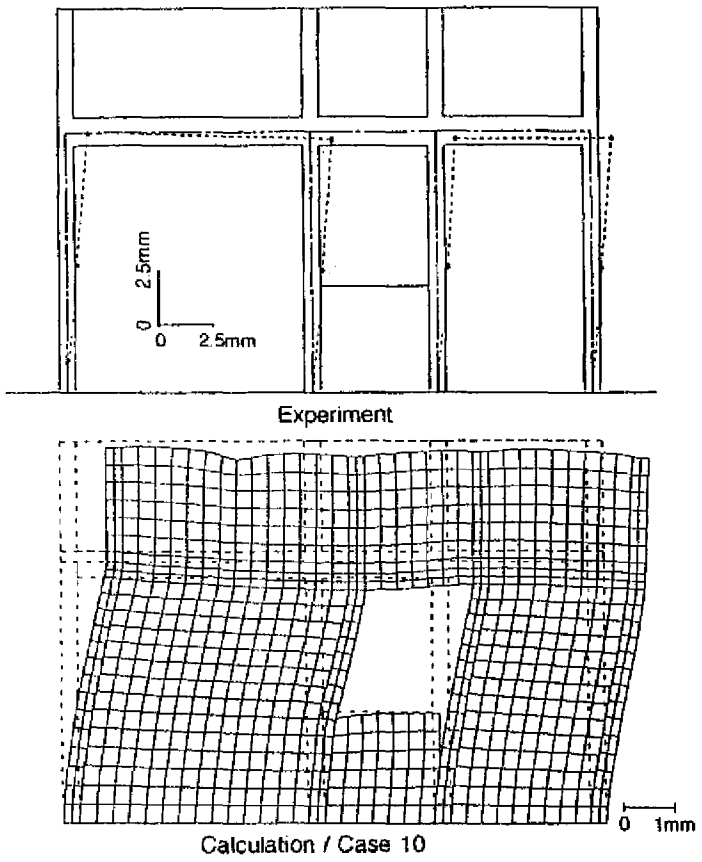

Fig. 7.3.2 Deformation pattern at a horizontal load of +18tf

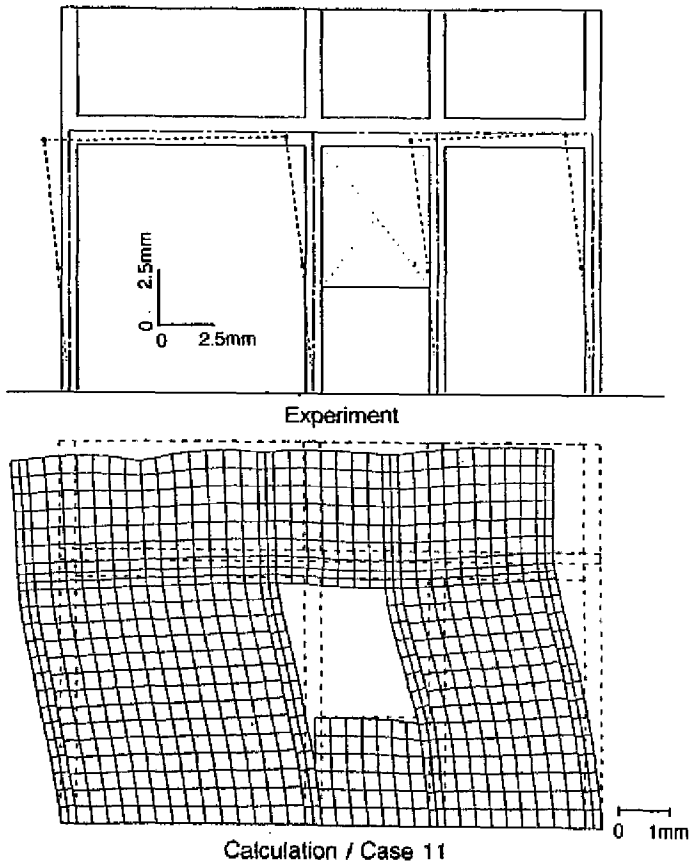

Fig. 7.3.3 Deformation pattern at a horizontal load of -18tf

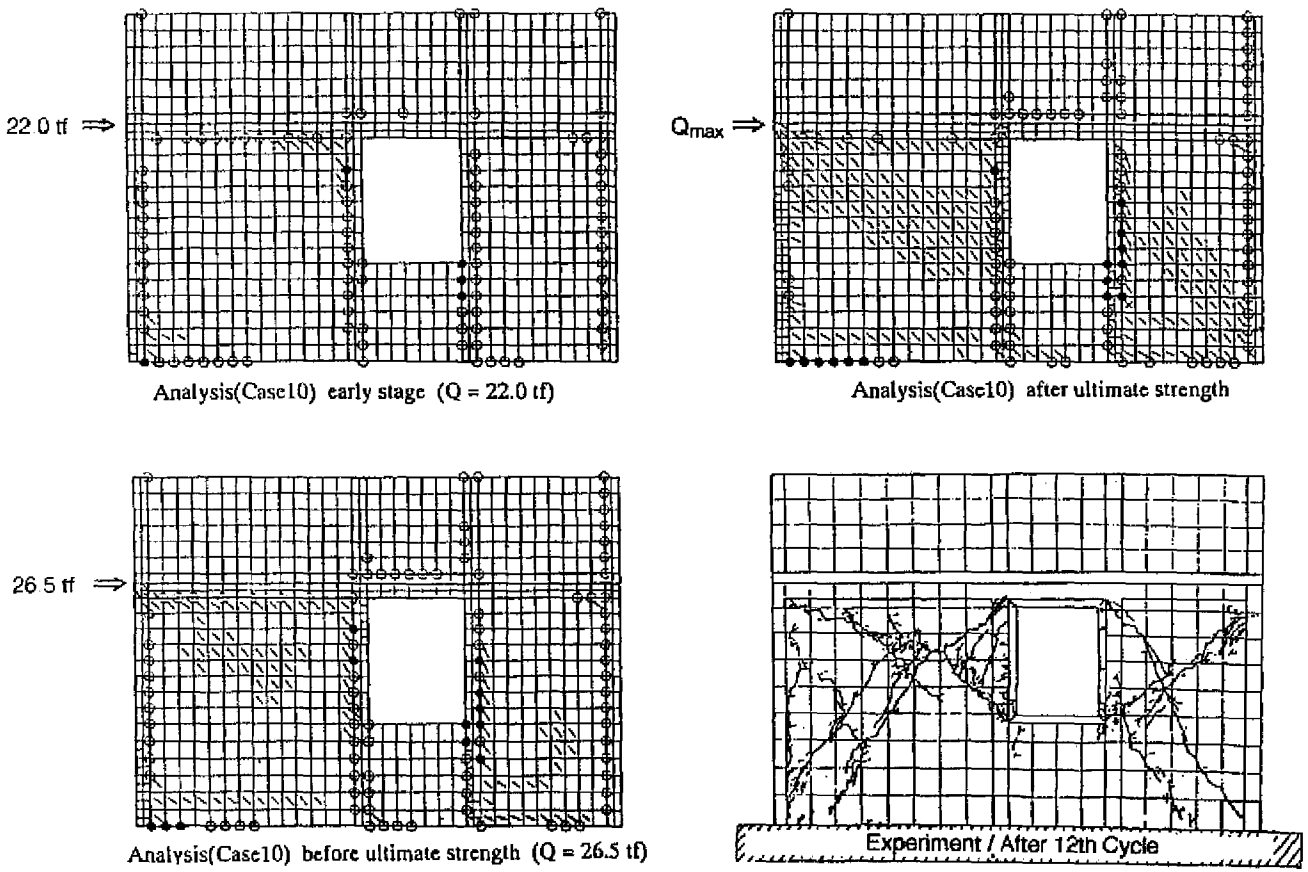

Fig. 7.3.4 Crack development in Case 10: WWW, positive loading, vertical load 25tf

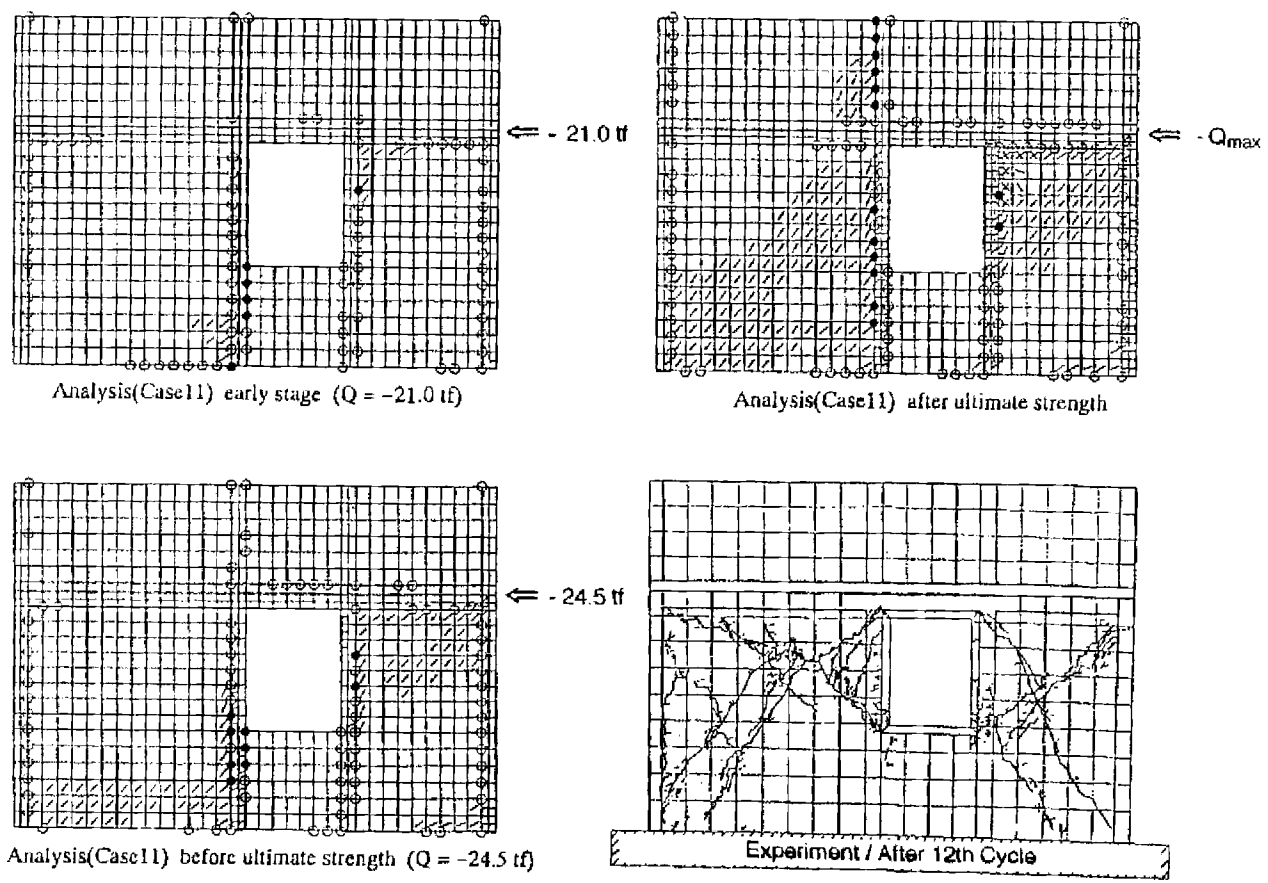

Fig. 7.3.5 Crack development in Case 11: WWW, negative loading, vertical load 25tf

7.4 Cases 12 and 13; Specimen WBW-E

Specimen WBW-E had the same geometry as Specimen WBW, but its brick walls were horizontally reinforced with a pre-fabricated ladder-shaped reinforcement. In Fig 7.4.1 the load-displacement relationships calculated in Case 12 and 13 are compared with test results Calculated load-displacement curves are in good agreement with test results in the drift angle range from -0 002 to +0 002. However, outside this range, a considerable difference between calculation and test results are observed The discrepancy is attributed to the fracture of the ladder-shaped reinforcement at a drift angle of around 0.002. Failure of horizontal reinforcement led to degradation of the load-displacement relation, but in the calculation such kind of fracture of reinforcement was not taken into consideration.

Looking at Table 7.4, a big difference in the values of ultimate shear strengths and corresponding drift angles are observed between computed and test results

Table 7.4 Ultimate shear strengths and corresponding drift angles in Cases 12 and 13

Case	Ultimate Shear Strength			Drift Angle at Ultimate Strength	
	Test (tf)	Cal. (tf)	Test/Cal.	Test (10^{-3})	Cal (10^{-3})
12	31.3	45.2	0.69	2.21	7.52
13	34.2	47.5	0.72	5.00	6.37

Crack development, including slips and separations, and crack patterns at the final stage compared with test results are shown in Figs 7.4.2 and 7 4.3 When ultimate strength was attained in the calculation, diagonal cracks propagate all over the brick walls and strain softening or concrete crushing occurred at wall corners. These are phenomena which did not appear in Specimen WBW (see Figs 7.1.6 to 7.1.9), and imply the effectiveness of horizontal reinforcement in brick masonry walls. Should the ladder-shaped reinforcement had not fractured in the experiment, the ultimate strength of Specimen WBW-E would have been larger.

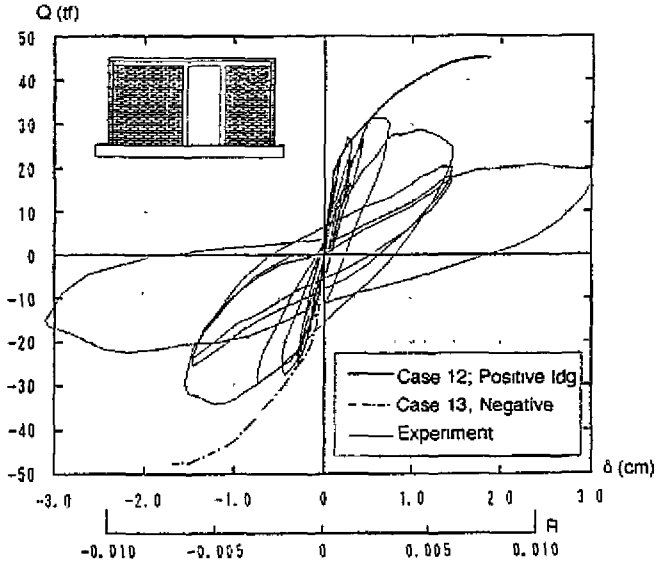

Fig. 7.4.1 Load (Q)-displacement (δ) relationships calculated in Case 12 and Case 13

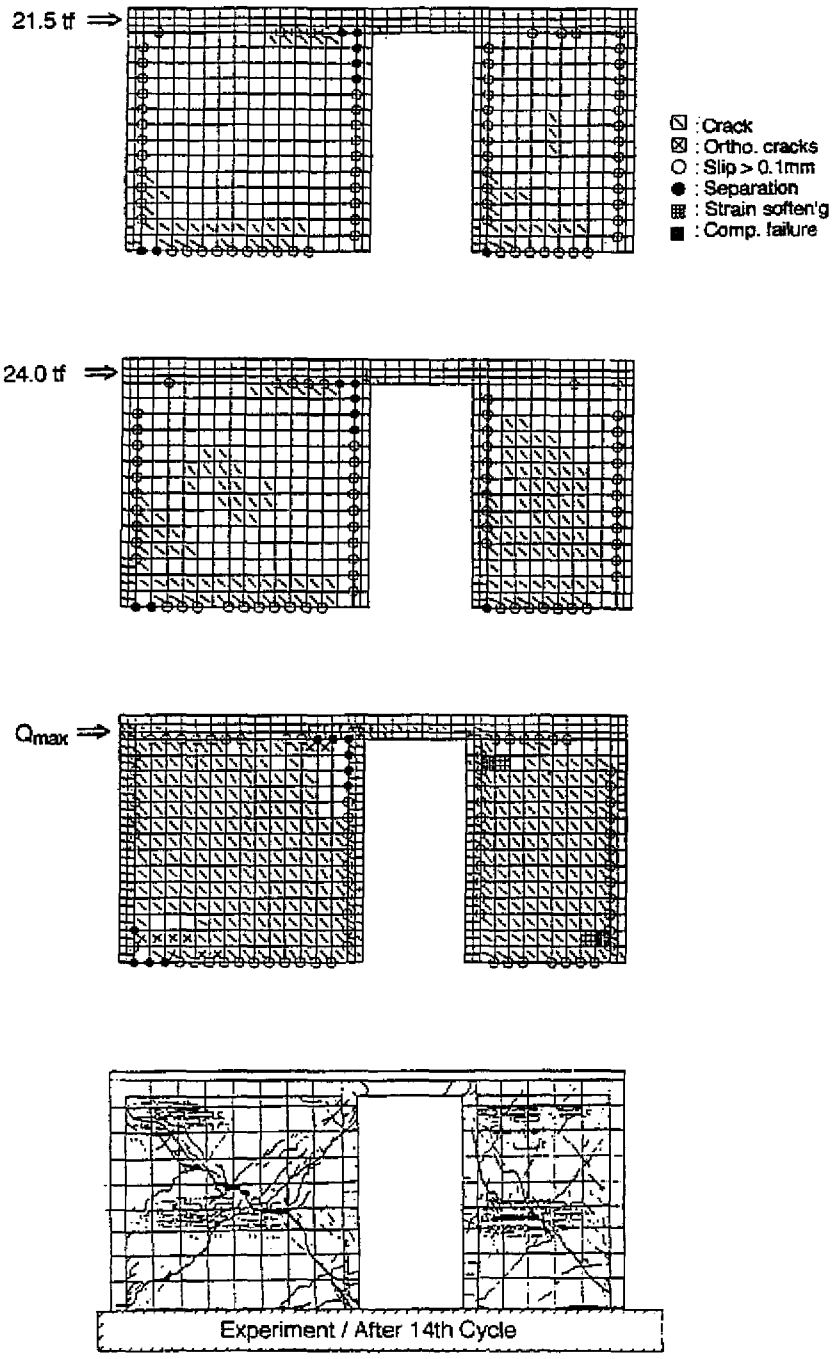

Fig. 7.4.2 Crack development in Case 12: WBW-E, positive loading, vertical load 25tf

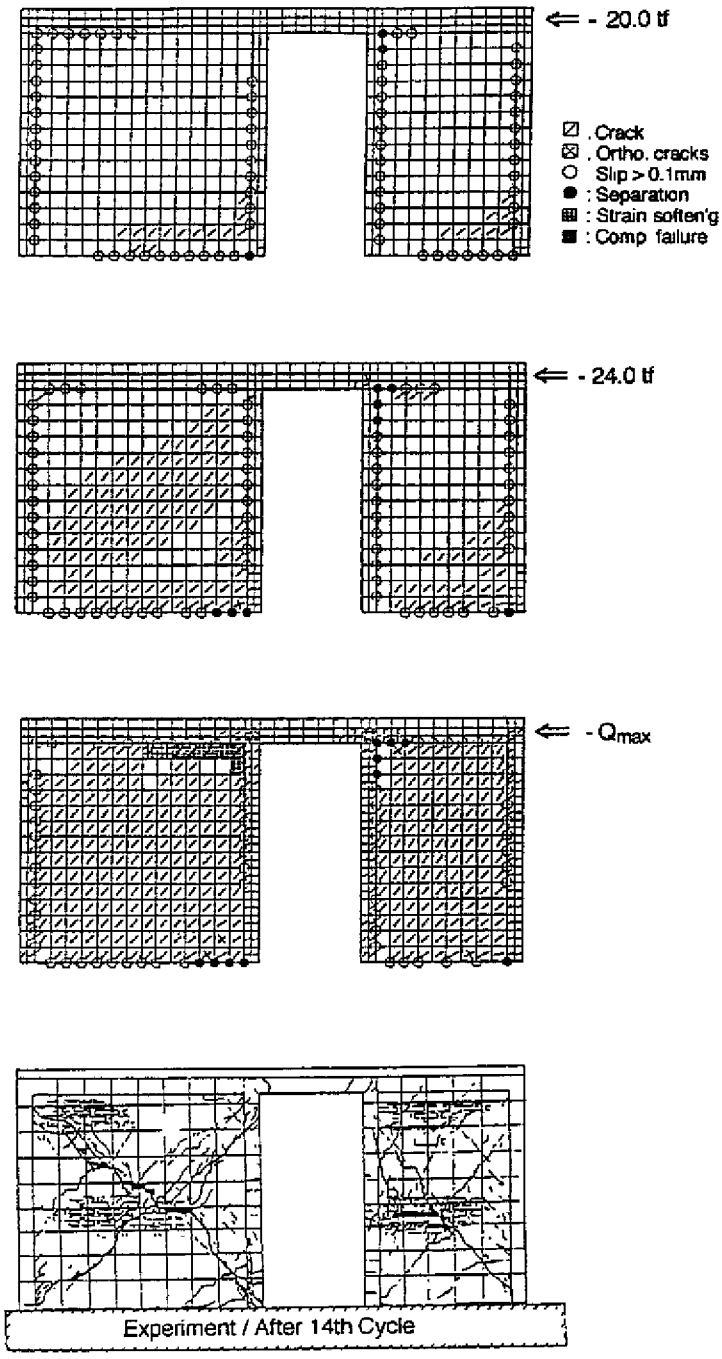

Fig. 7.4.3 Crack development in Case 13: WBW-E, negative loading, vertical load 25tf

7.5 Cases 14 to 19; Specimen WBW-B

Specimen WBW-B had also the same geometry as Specimens WBW and WBW-E, but walls were horizontally reinforced with two high-strength cold-drawn deformed wires at every three courses. The summary of analyses results and their comparison with test results are presented in Table 7.5.

In Fig. 7.5.1 the load-displacement relationships calculated in Cases 14 and 15 are shown and are compared with the test results. In Case 14, the calculated relation agrees well with the test results, though the elastic rigidity and displacement at ultimate strength were a little larger than those measured in the experiments. Calculated values of ultimate shear strength and displacement at ultimate strength in Case 15 were larger than test results by about 20%. Effects of loading sequence of horizontal force are clearly observed in the range of horizontal load over 30tf, where shear rigidity and shear resistance in the negative loading (Case 15) are larger than those in positive loading (Case 14).

Table 7.5 Ultimate shear strengths and corresponding drift angles in Cases 14 to 19

Case	Ultimate Shear Strength			Drift Angle at Ultimate Strength	
	Test (tf)	Cal. (tf)	Test/Cal.	Test (10^{-3})	Cal. (10^{-3})
14	46.8	46.1	1.02	7.41	10.43
15	41.1	50.5	0.81	6.01	8.91
16	-	46.1	-	-	7.32
17	-	44.5	-	-	8.17
18	46.8	44.5	1.05	7.41	8.32
19	41.1	43.7	0.94	6.01	4.96

The effect of vertical load on the load-displacement relationship are observed in Fig. 7.5.2, where the curves for Cases 14, 16 and 17 are compared: as in other specimens, vertical load did not greatly affect the elastic rigidity but it increased the ultimate strength and the stiffness in the plastic range.

In Fig. 7.5.3, the load-displacement curves for Case 14 (monotonic positive loading) and for Case 18 (cyclic loading) are compared. A similar comparison is shown in Fig. 7.5.4, for Case 15 (negative monotonic loading) and Case 19 (cyclic loading). In Case 18, horizontal load was applied up to 20tf in the negative direction first, then unloaded to zero, and finally reloaded in the positive direction to the ultimate state. On the other hand, in Case 19, horizontal load is applied up to 20tf in the positive direction first, then unloaded to zero, and finally reloaded in the negative direction up to the ultimate state. In Fig. 7.5.3, slight difference is observed at displacements larger than 1.5 cm between Cases 14 and 18. In Fig. 7.5.4, it is observed that the cyclic loading and loading sequence contribute to reduce the shear rigidity in the plastic region, ultimate shear strength and ductility.

In Figs 7.5.5 to 7.5.10 the crack development (including slips and separation) and crack patterns at the final stage compared with test results are shown. When ultimate strength was attained in the analysis, inclined cracks propagated over the brick walls and strain softening or concrete crushing occurred at wall corner. The details of the crack patterns can be seen on Fig. 7.5.11, where crack patterns for Case 1 are also shown for comparison. These results are in good agreement with the test results. Horizontal wires in brick masonry walls of this test specimen also fractured in the experiment as in the case of Specimen WBW-E. However, fracture occurred at a drift angle larger than 0.006 after steel plastification. This is considered the reason why the analyses results for Specimen WBW-B are very similar to the behavior observed in the experiment.

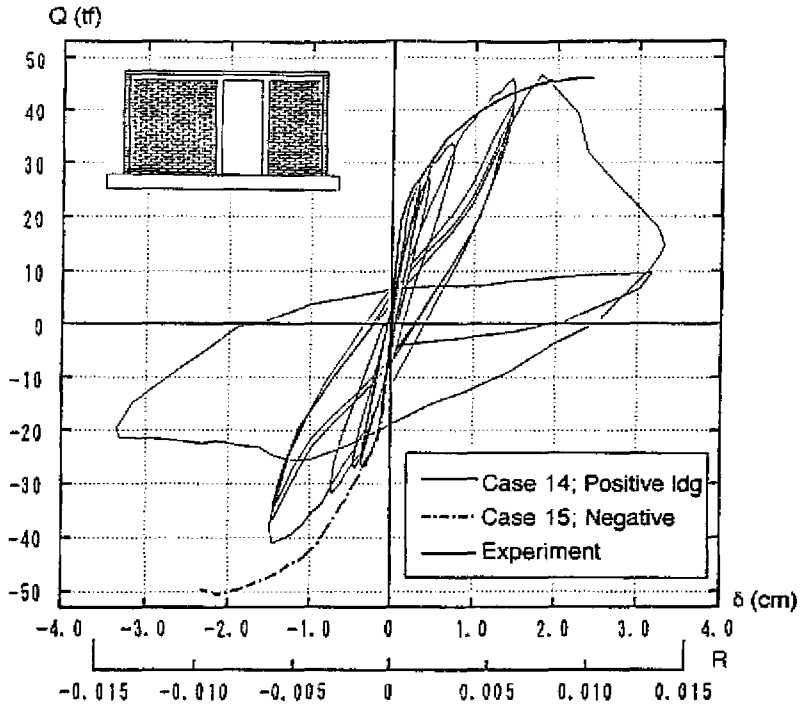

Fig. 7.5.1 Load (Q)-displacement (δ) relationships calculated in Case 14 and Case 15

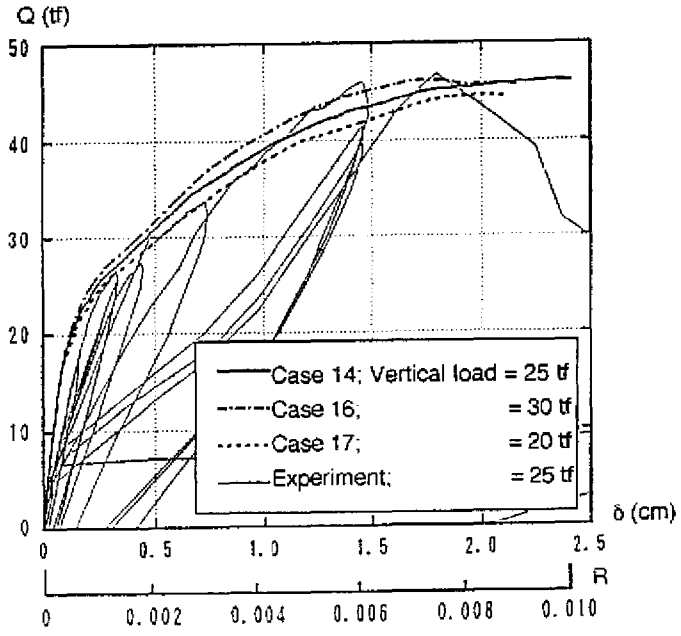

Fig. 7.5.2 Load (Q)-displacement (δ) relationships calculated in Case 14, Case 16 and Case 17

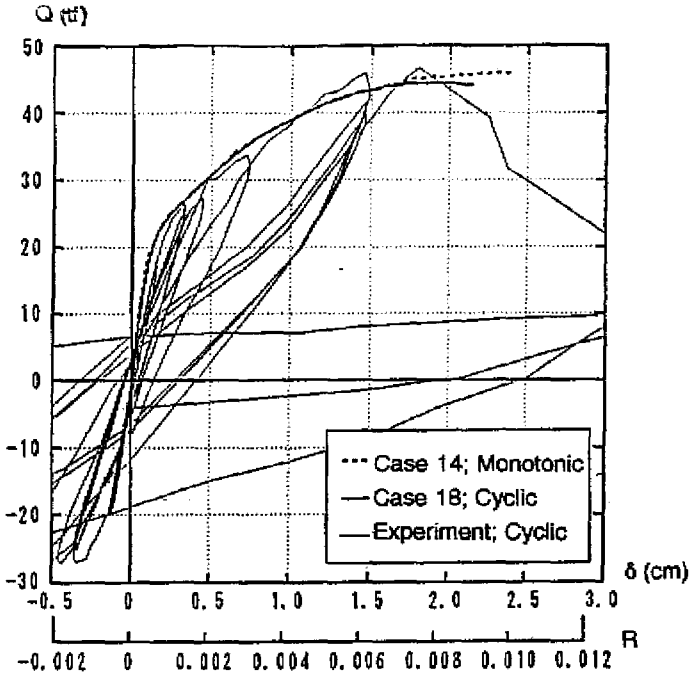

Fig. 7.5.3 Load (Q)-displacement (δ) relationship calculated in Case 14 and Case 18

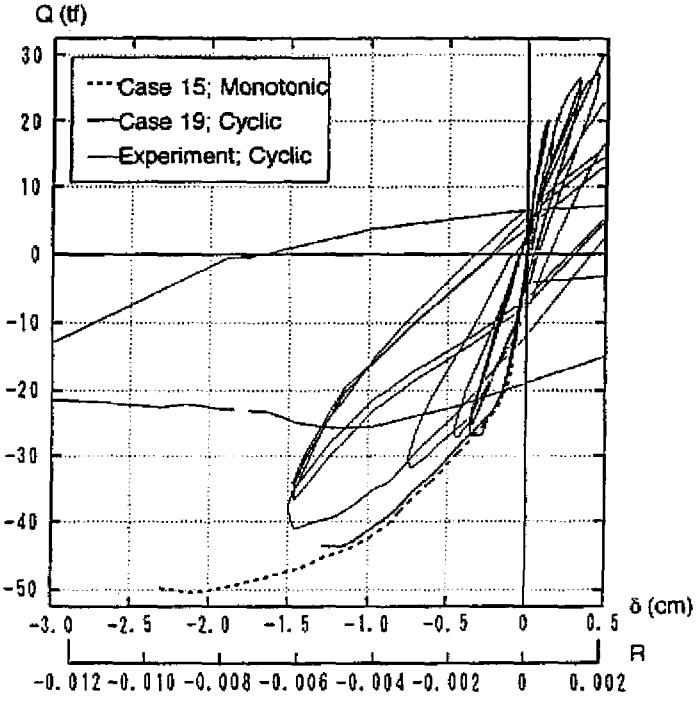

Fig. 7.5.4 Load (Q)-displacement (δ) relationship calculated in Case 15 and Case 19

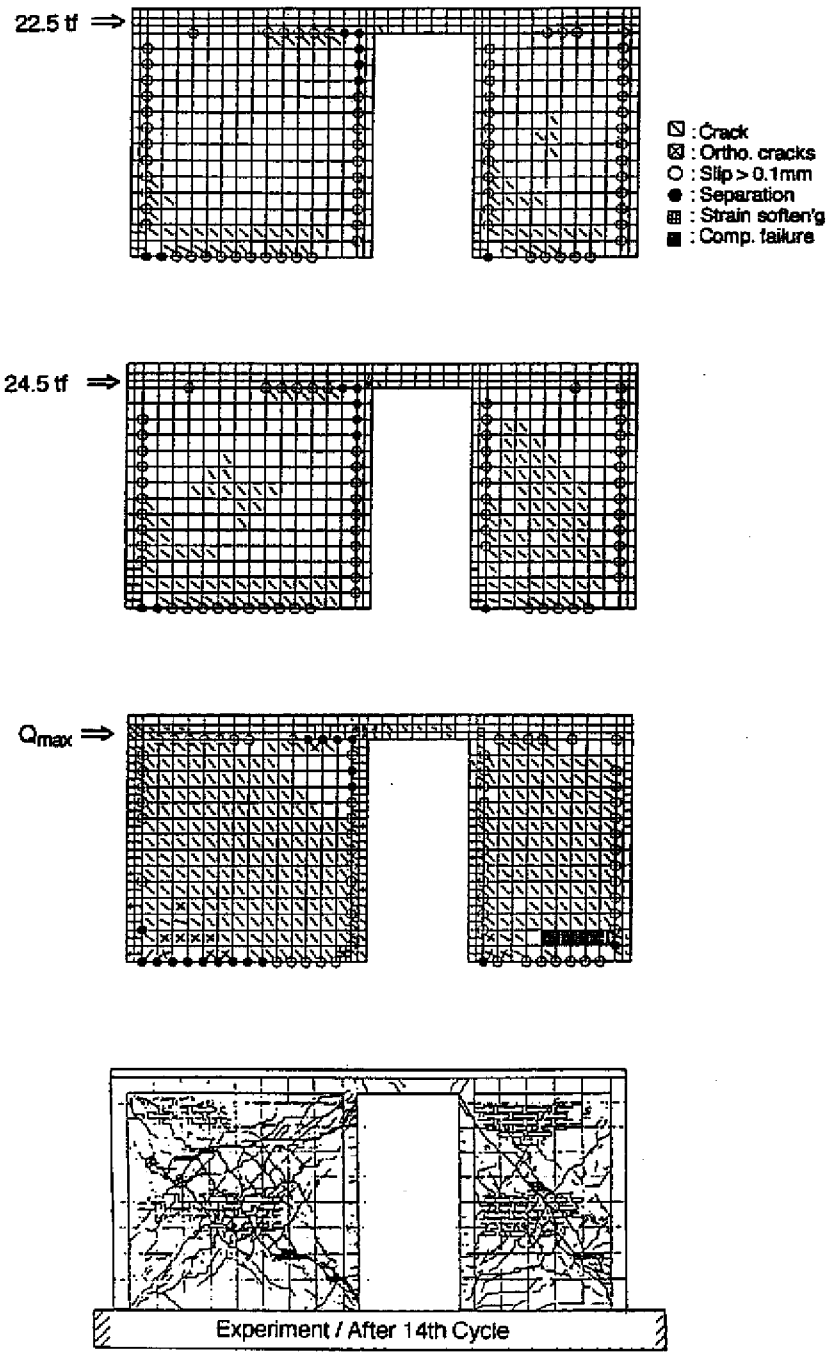

Fig. 7.5.5 Crack development in Case 14: WBW-B, positive loading, vertical load 25tf

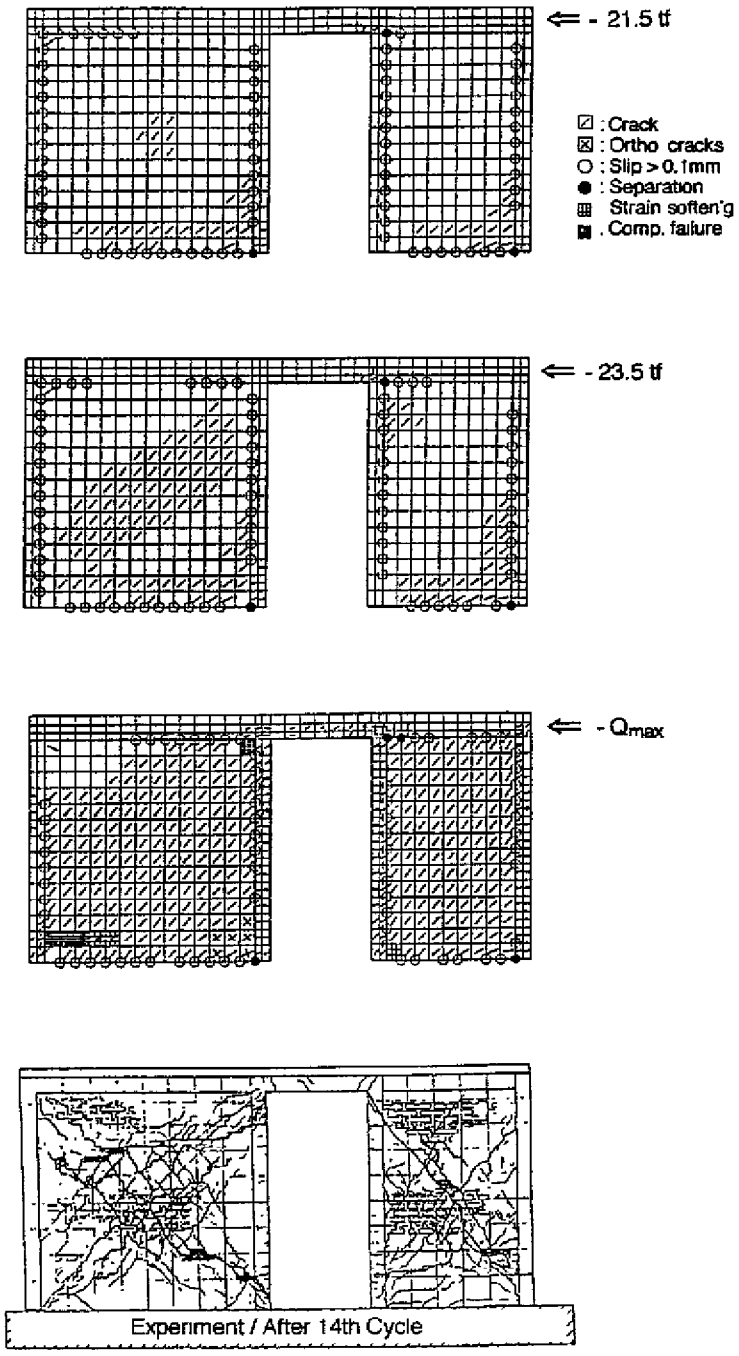

Fig. 7.5.6 Crack development in Case 15: WBW-B. negative loading, vertical load 25tf

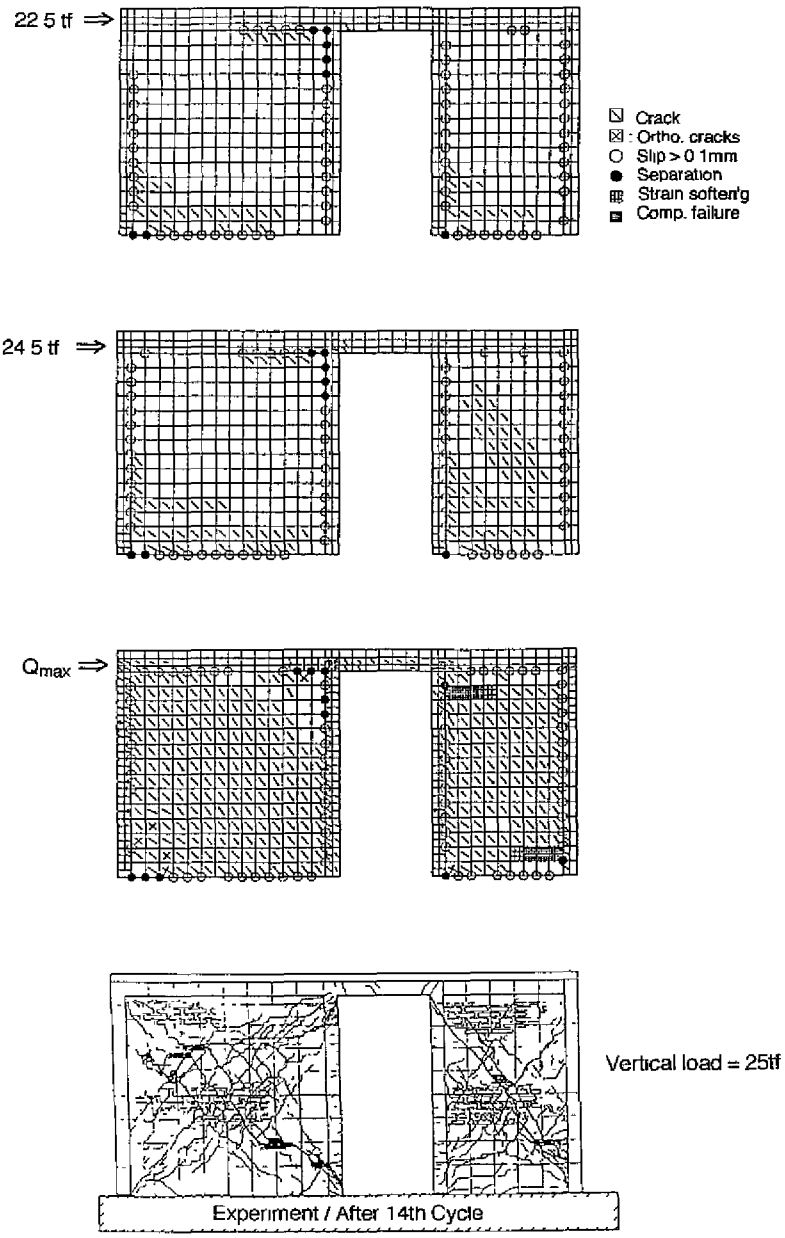

Fig. 7.5.7 Crack development in Case 16· WBW-B, positive loading, vertical load 30tf

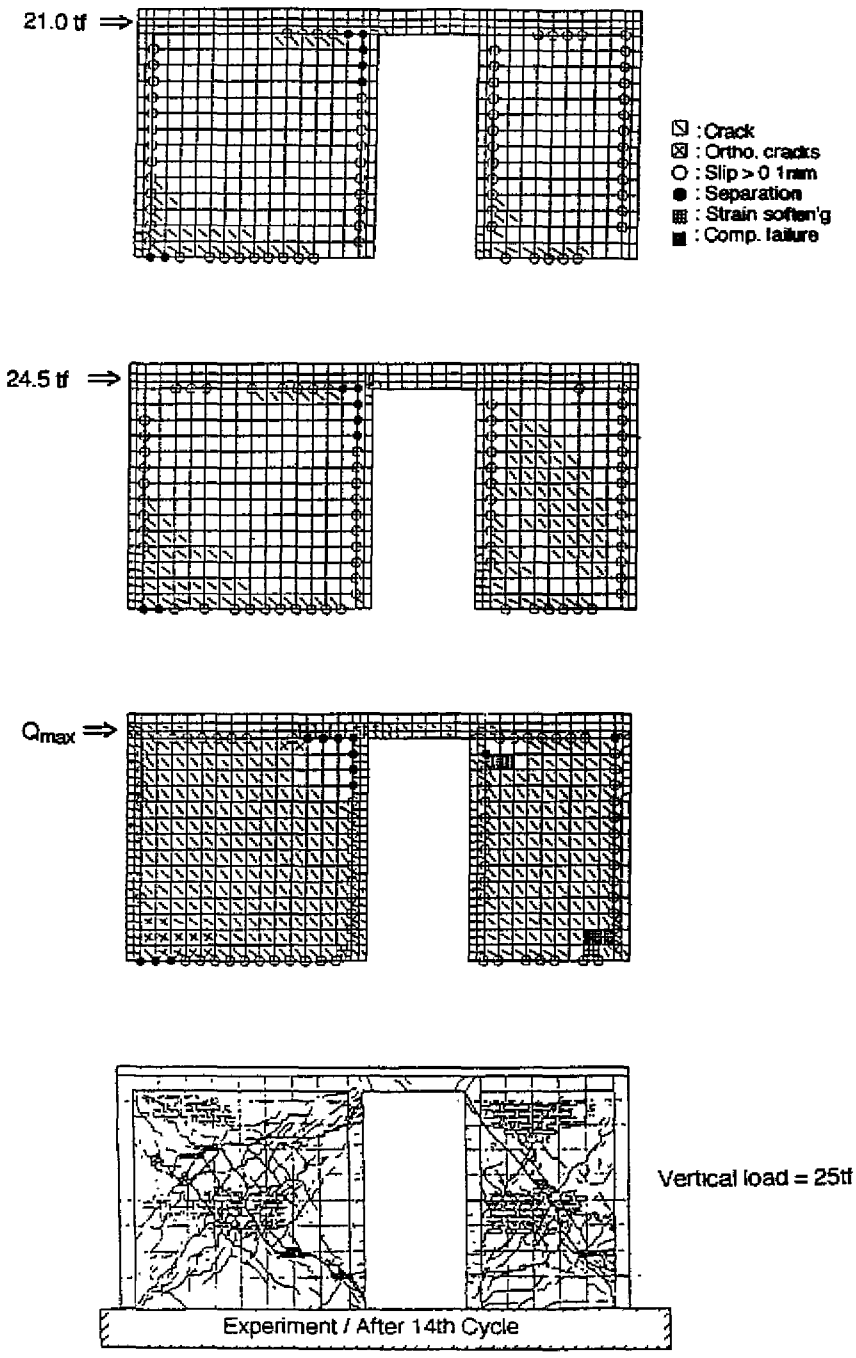

Fig. 7.5.8 Crack development in Case 17: WBW-B, positive loading, vertical load 20tf

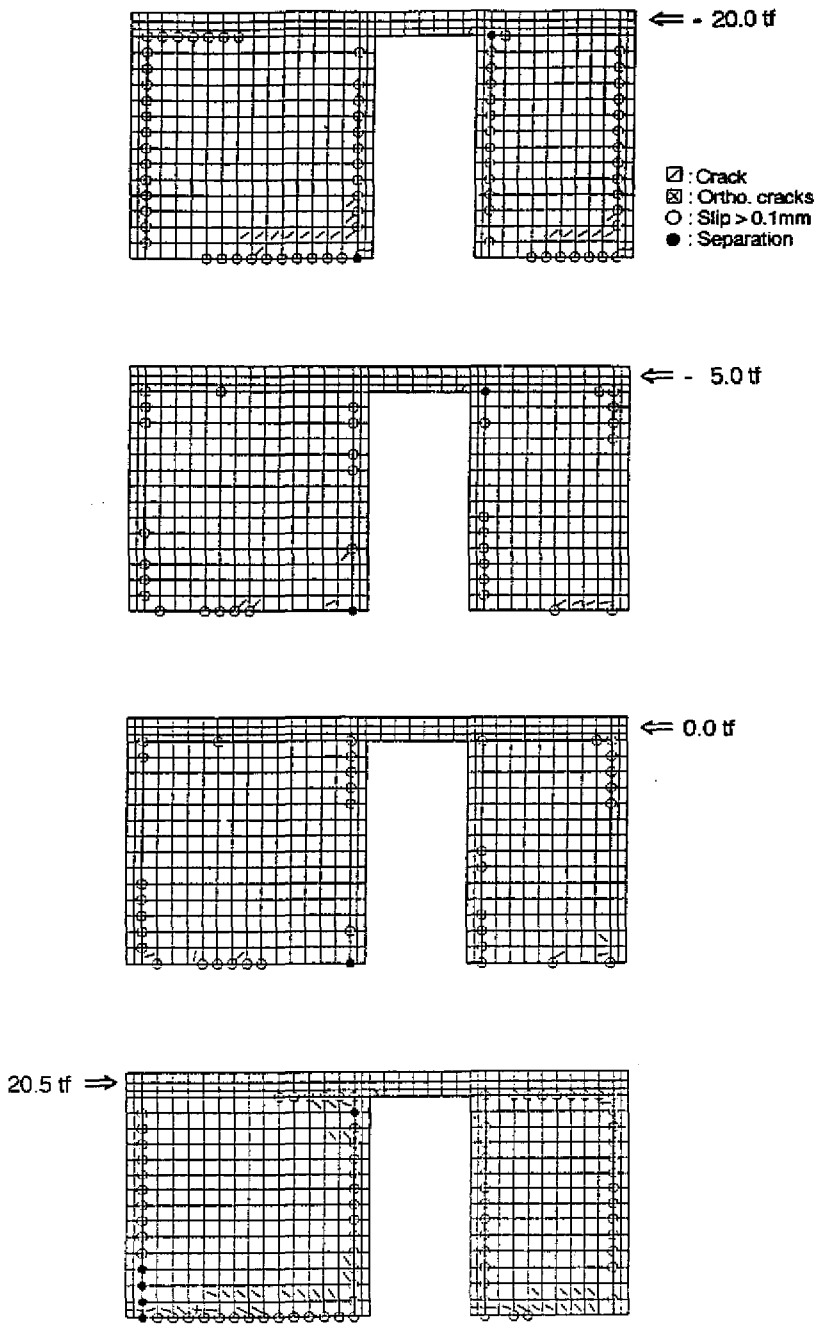

Fig. 7.5.9 (a) Crack development in Case 18: WBW-B, positive loading, vertical load 25tf, cyclic loading

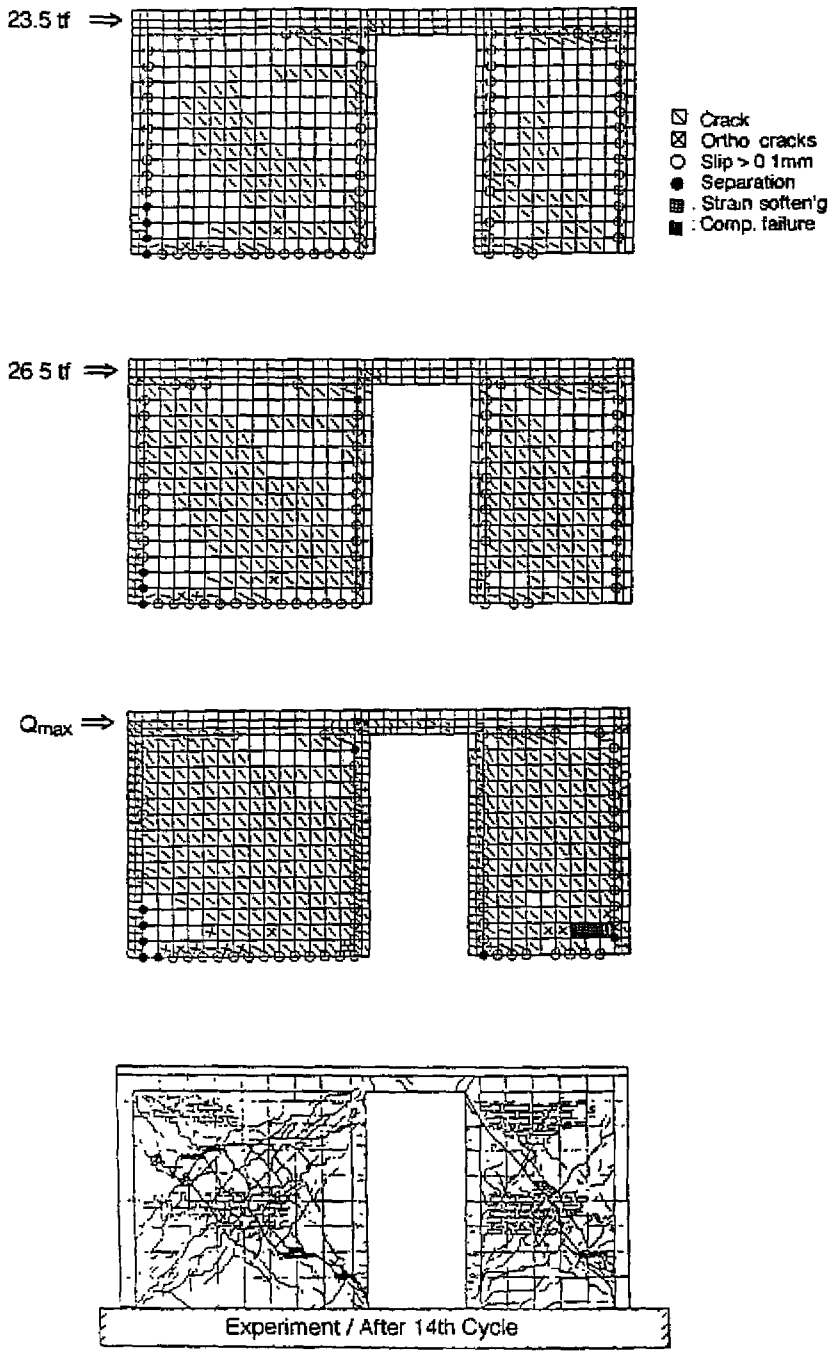

Fig. 7.5.9 (b) Crack development in Case 18: WBW-B, positive loading, vertical load 25tf, cyclic loading

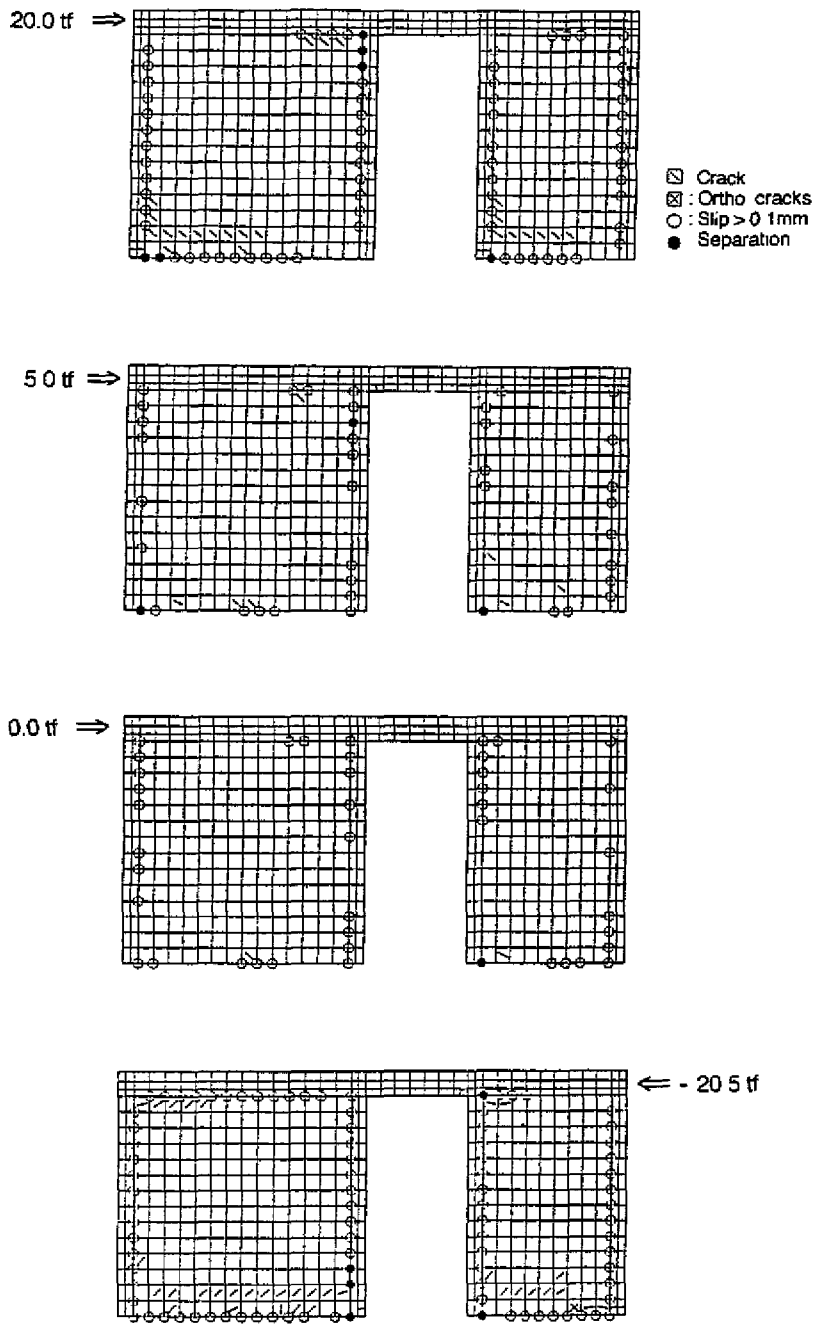

Fig 7.5 10 (a) Crack development in Case 19: WBW-B, negative loading, vertical load 25tf, cyclic loading

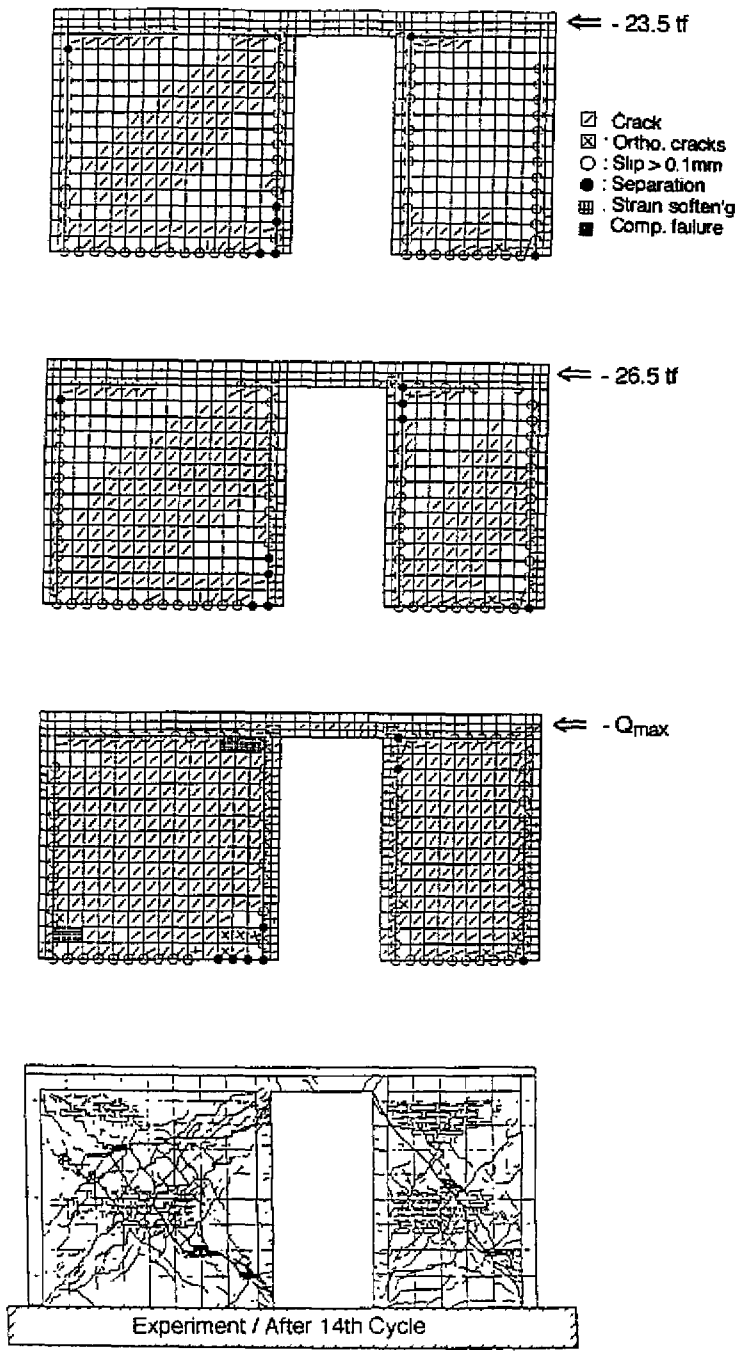

Fig. 7.5.10 (b) Crack development in Case 19: WBW-B, negative loading, vertical load 25tf, cyclic loading

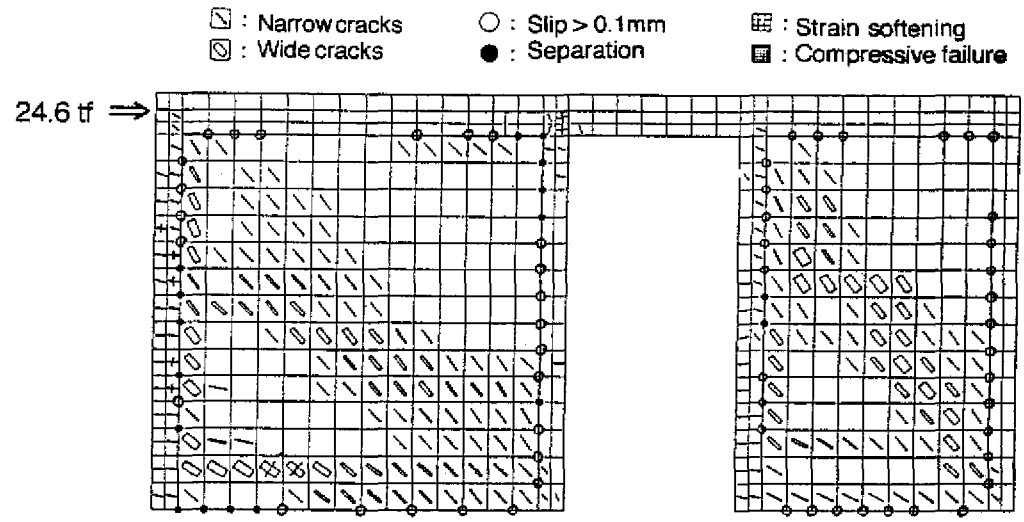

(a) Specimen WBW / No reinforcement in masonry walls / Case 1

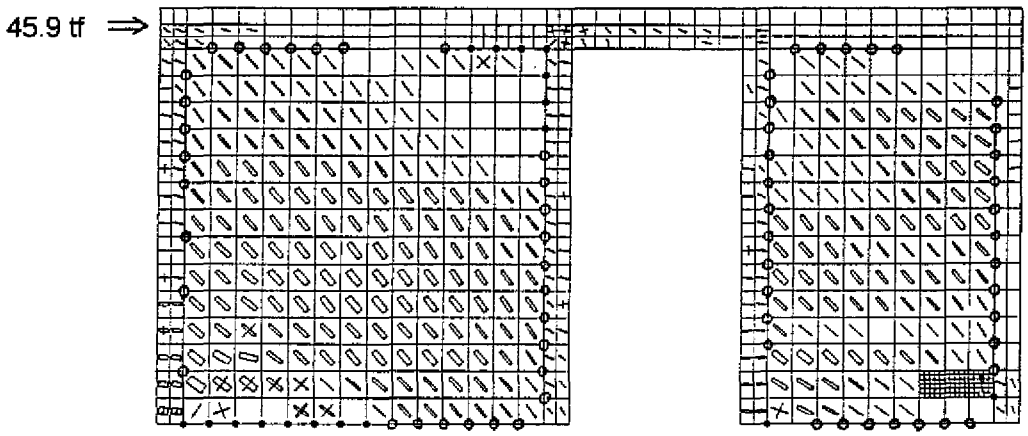

(b) Specimen WBW-B / Horizontal reinforcement in masonry walls / Case 14

Fig. 7.5.11 Comparison of cracking patterns of Case 1 and Case 14

8. CONCLUSION

In this paper, the finite element method was applied to the analysis of confined masonry structures subjected to horizontal loads. Results of the experiments on full-scale confined masonry walls conducted at CENAPRED in 1991 to 1992, were utilized for investigating the validity of the application.

The most critical point when applying the finite element method to confined masonry structures is the selection of suitable analytical models which represent the mechanical characteristics of the boundary between the reinforced concrete structural members and the brick masonry walls. In this paper, coupling elements on the boundary, each of which has two springs in the directions normal and parallel to the boundary surface were used. The spring in the direction parallel to the boundary surface had a spring constant which depended on the magnitude of normal stress acting on the boundary surface.

The horizontal load-horizontal displacement relationships calculated were, in general, in good agreement with the test results. In some cases, the analyses did not correlate with the test results well. This was attributed to an inadequate modeling of the boundary conditions.

In the analyses presented, convergence of solutions in every step of calculation was not complete, but at this time there is no analytical solution to prevent this problem.

ACKNOWLEDGEMENT

This research is conducted as a part of the CENAPRED-JICA (Japan International Cooperation Agency) cooperative program on the earthquake disaster prevention.

The authors express their sincere thanks to Dr. Roberto Meli, Research Director, CENAPRED, Dr. Sergio M. Alcocer, Head of the Seismic Test Area, Research Department, CENAPRED, Mr. Lorenzo D. Sanchez and Mr. Tomas Sanchez, Researchers, Research Department, CENAPRED, for their effort in conducting the experiments on confined masonry structures and also for offering the data of this research. Mr. Motoji Saito, a former Japanese expert dispatched to CENAPRED from 1991 to 1992, provided information and data on the material characteristics of confined masonry structures. Many thanks are extended to him.

REFERENCES

1) Ishibashi, K., R Meli, S.M. Alcocer, F. Leon and T.A Sanchez (1992). Experimental study on earthquake-resistance design of confined masonry structures, *Proceedings of 10WCEE*, Madrid, Vol. 6, pp 3469-3474.

2) Ishibashi, K and H. Kanemaru (1992) Seismic tests of confined masonry structures using solid clay bricks in Mexico (Part 1) (Part 2), *Proc. of Annual Conv., Struct. II*, AIJ, pp. 1969-1972, (in Japanese).

3) Darwin, D. and D.A Pecknold (1977). Nonlinear biaxial stress-strain law for concrete, *Journal of the Engineering Mechanics Division*, ASCE, Vol. 103, No EM2, pp. 229-241.

4) Kupfer, H.B and K.H. Gerstle (1973). Behavior of concrete under biaxial stress, *Journal of the Engineering Mechanics Division*, ASCE, Vol. 99, No. EM4, pp. 853-866.

5) Fafitis, A. and S P. Shah (1985). Lateral reinforcement for high-strength concrete columns, *ACI Special Publication*, No. SP-87, pp. 213-232.

6) Departamento del Distrito Federal (1989). Normas Tecnicas Complementarias para Diseño y Construcción de Estructuras de Mampostería. *Gaceta Oficial del Departamanto del D.F.*, p. 19.

7) Fujii, K., T. Kubo, H. Katsumata, et al. (1990). Evaluation of seismic capacity and retrofit of an existing brick masonry structure (Part 1 - 4), *Proc. of Annual Conv., Struct. II*, AIJ, pp. 1009-1016, (in Japanese).

8) Amemiya, A. and H. Noguchi (1990). Development of finite element analytical program of high strength reinforced concrete members (Part 1: Development of concrete model), *Proc. of Annual Conv., Struct. II*, AIJ, pp. 639-640, (in Japanese).

9) State-of-the art report on high strength concrete (1991), chapter 2, 3.3.1; Tensile strength: edited by AIJ, (in Japanese)

APPENDIX: Preliminary Analysis on Modeling of the Boundary Element between Brick Masonry Walls and Peripheral Concrete Frames

Typical mechanical properties of confined masonry structures are:

1) mechanical discontinuity at the boundary surface between brick masonry walls and the confining reinforced concrete members (tie-columns and bond-beams),
2) non-homogeneity of masonry walls which consist of bricks and joint mortar,
3) brittle nature of the failure mode of masonry walls since horizontal wall reinforcement is not provided, and
4) large variation of material characteristics

which are major factors that make the theoretical analysis very difficult.

According to the authors' preliminary investigation, the first property, that is mechanical discontinuity at the reinforced concrete and brick boundary, has the most critical effects on crack development and load-displacement relations of confined masonry structures. In this paper, the authors adopted a two-spring linkage element as an equivalent of the property of this boundary surface. In this appendix, the preliminary analysis, which served as basis for the two-spring linkage element assumed in this paper, is described.

A1. Concept of Two-Spring Linkage Element

At the boundary surface brick masonry walls and confining reinforced concrete members (hereinafter, boundary surface), separation and slippage have to be taken into consideration in the analysis When analyzing reinforced concrete structures, two-spring linkage elements are used in order to simulate the behavior of discrete cracks. The concept of this linkage element is shown in Fig. A1. The element consists of two orthogonal springs, one of which is effective in the direction normal to the boundary surface (normal spring) and the other is effective in the direction parallel to the boundary surface (parallel spring). Normal and parallel springs represent the behavior of separation and slippage, respectively Authors tried to apply this linkage element to confined masonry structures.

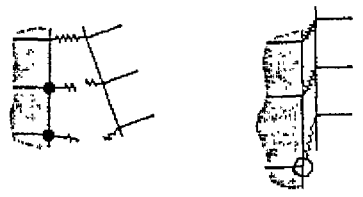

(a) Separation (b) Slippage

Fig. A1 Concept of linkage element

A2. Cut-off Strength of Normal Springs

The normal spring has to be cut off when the stress acting on the spring exceed the bond strength of the boundary surface σ_r. However, the bond strength σ_r was not measured in the experiment, and so three cases of calculations were conducted with reference to the test results for Specimen WBW, supposing $\sigma_r = \infty$ (Case A), 0.0 kgf/cm^2

(Case B) and 5.4 kgf/cm^2 (Case C). Here, 5.4 kgf/cm^2 in Case C is the tensile strength of bricks obtained from bending tests.

Table A1 and Figs A2 and A3 show the results of calculation, where the following can be observed:

1) There is very little difference in load-displacement relationships and ultimate shear strengths for Case A and Case C.
2) In Case A and Case C, calculated elastic rigidities are larger than the test results and calculated ultimate strengths are smaller than the test results.
3) In Case B, the calculated elastic rigidity is in good agreement with the test results but the stiffness in the plastic region and displacement corresponding to the ultimate strength are too small or too large compared with the test results, respectively.
4) Crack patterns ad deformation modes are not well simulated in all cases.

As a result, the cut-off strength of 5.4 kgf/cm^2 may be too large and a little smaller values should be better to be supposed However, no data is available to select an appropriate cut-off strength at this time. If 5.4 kgf/cm^2 is assumed as a cut-off strength, the elastic rigidity will probably be estimated at a larger value than the true value.

Table A1 Ultimate shear strengths and corresponding drift angles in Cases A to C

Case	σ_t (kgf/cm^2)	Ultimate Shear Strength			Drift Angle at Ultimate Strength	
		Test (tf)	Cal. (tf)	Test/Cal.	Test (10^{-3})	Cal. (10^{-3})
A	∞	26 4	23.5	1.12	1.35	0.85
B	0.0	26.4	26.3	1.00	1.35	2.32
C	5.4	26.4	23.5	1.12	1.35	0.84

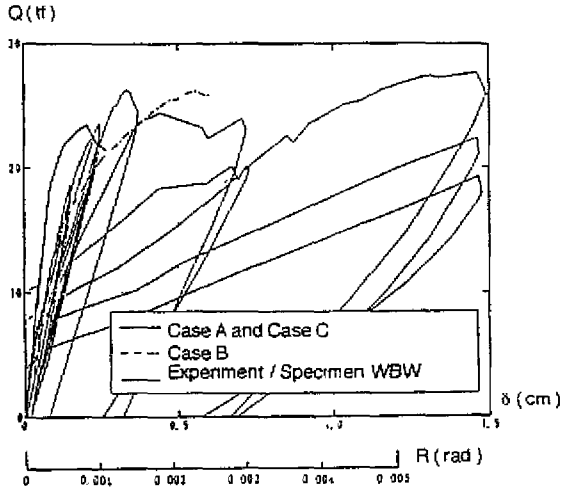

Fig. A2 Load (Q)-displacement (δ) relationships in Case A, Case B and Case C

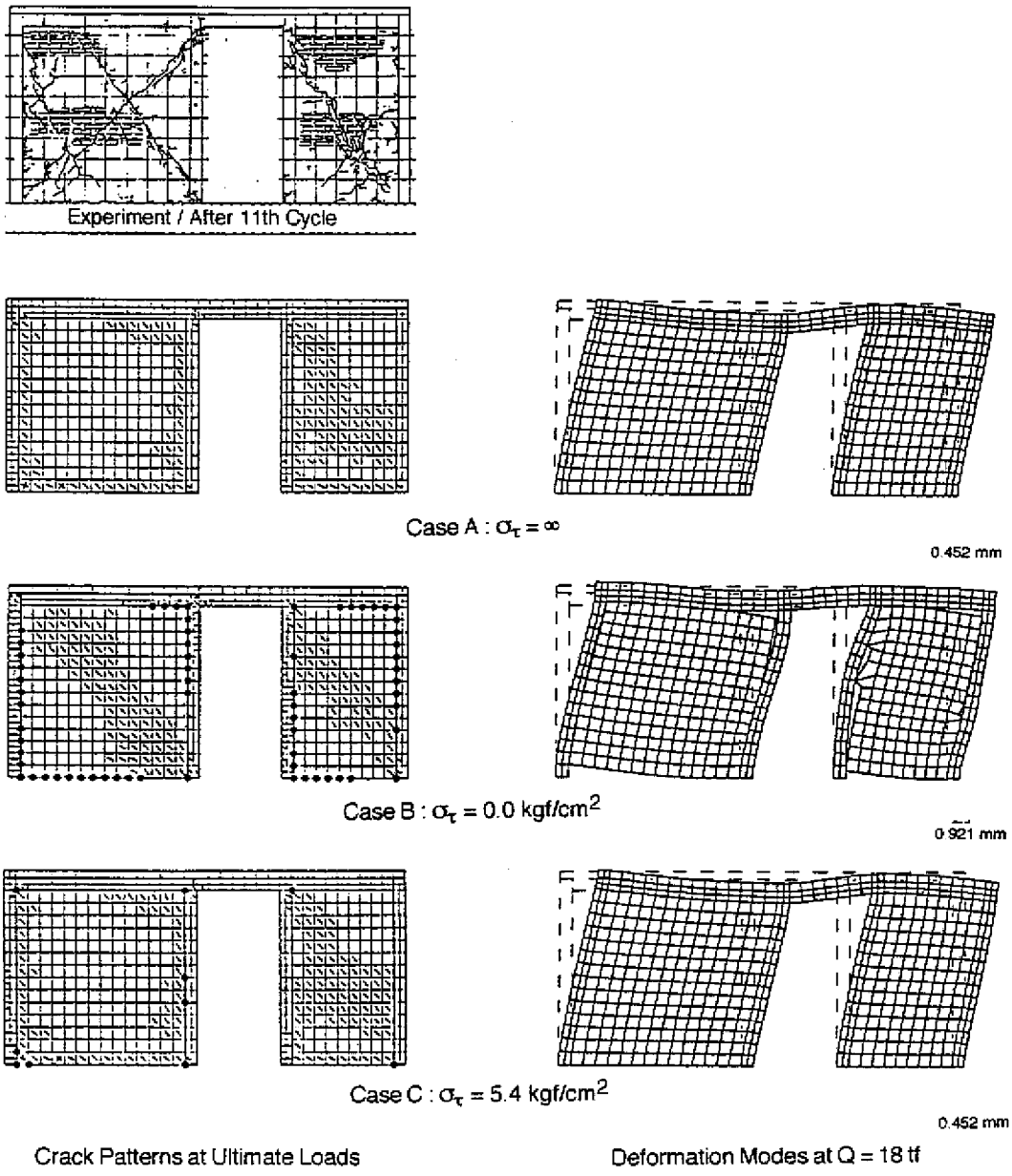

Fig. A3 Crack patterns and deformation modes in Case A, Case B and Case C

A3. Shear Stress-Shear Slip Relation for Parallel Springs

Two kinds of models were assumed in order to simulate the slip phenomenon as shown in Fig. A4. The shear stress-shear slip relation is assumed to be bi-linear in both cases, but the trigger shear stress, at which the slip occurs, was fixed at 9.2 kgf/cm^2 (this value is selected from the test results in Ref. 7) in Model-1, and in case of Model-2 it was assumed to be a function of the normal stress acting at the boundary surface.

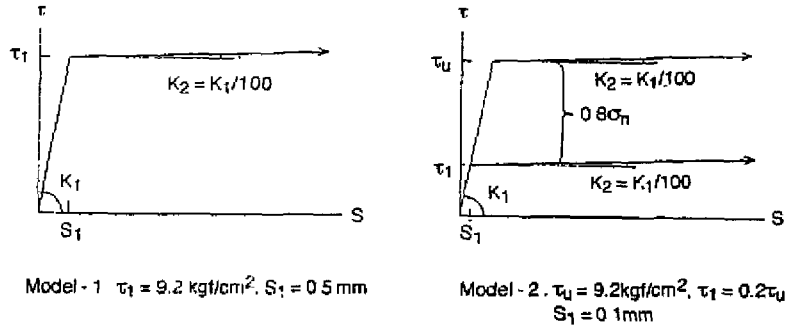

Fig A4 Shear stress (τ)-shear slip (S) relationship at the boundary

Two cases of calculations (Case D and Case E) were conducted in order to simulate the test results on test specimen WBW in the experiment, assuming these two models. In the calculations, the cut-off strength of normal springs was supposed to be 5.4 kgf/cm^2.

Results are shown in Table A2, Figs A5 and A6. Observing these results, it looks that Model 2 can simulate the behavior better than Model 1.

Table A2 Ultimate shear strengths and corresponding horizontal displacements in Cases D and E

Case	Slip Model	Ultimate Shear Strength			Drift Angle at Ultimate Strength	
		Test (tf)	Cal. (tf)	Test/Cal.	Test (10^{-3})	Cal (10^{-3})
D	Model 1	26.4	24.8	1.06	1.35	1.59
E	Model 2	26.4	23.5	1.12	1.35	0.84

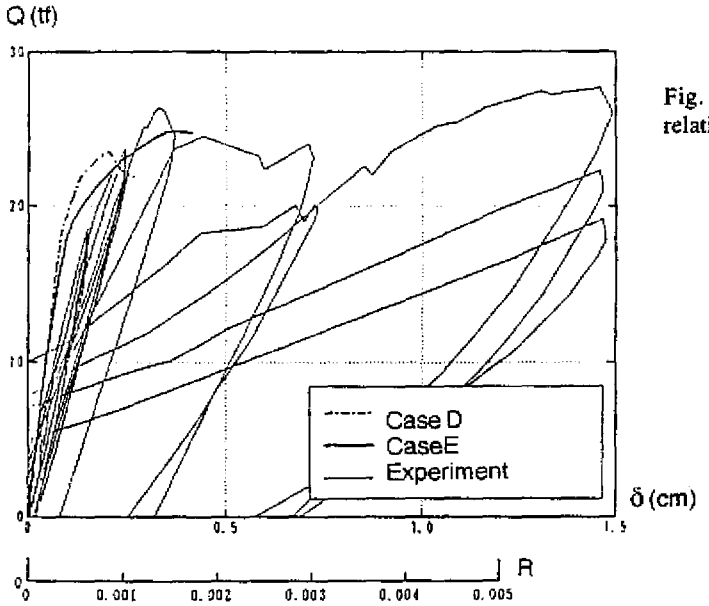

Fig. A5 Load (Q)-displacement (δ) relationships in Case D and Case E

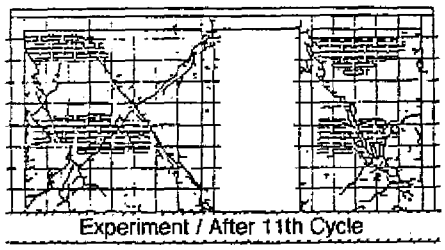

Fig. A6 Crack patterns and deformation modes in Case D and Case E

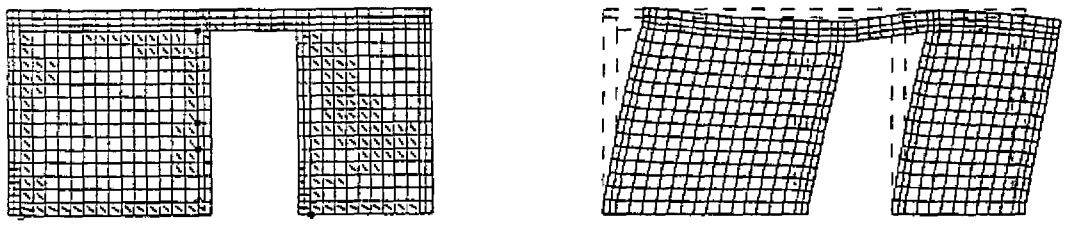

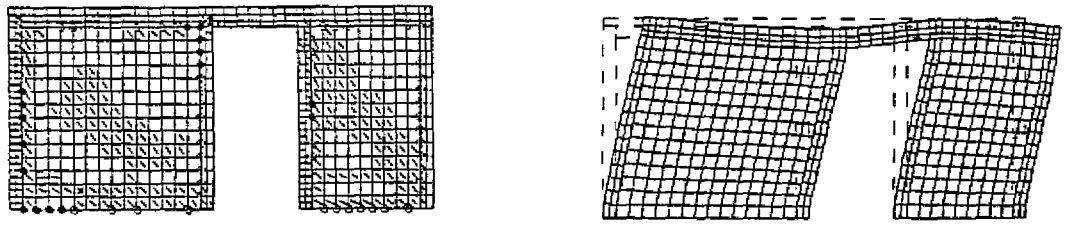

Crack Patterns at Ultimate Loads

Deformation Modes at Q = 18 tf

TITULOS PUBLICADOS

BASES DE DATOS PARA LA ESTIMACION DE RIESGO SISMICO EN LA CIUDAD DE MEXICO; Coordinación de Investigación; Area de Riesgos Geológicos; M. Ordaz, R. Meli, C. Montoya-Dulché, L. Sánchez y L.E. Pérez-Rocha.

TRANSPORTE, DESTINO Y TOXICIDAD DE CONSTITUYENTES QUE HACEN PELIGROSO A UN RESIDUO; Coordinación de Investigación; Area de Riesgos Químicos; Ma. E. Arcos, J. Becerril, M. Espíndola, G. Fernández y Ma. E. Navarrete.

PROCESOS FISICOQUIMICOS PARA ESTABILIZACION DE RESIDUOS PELIGROSOS; Coordinación de Investigación; Area de Riesgos Químicos; M. Y. Espíndola y G. Fernández.

REFLEXIONES SOBRE LAS INUNDACIONES EN MEXICO; Coordinación de Investigación; Area de Riesgos Hidrometeorológicos; R. Domínguez, M. Jiménez, F. García y M.A. Salas.

MODELO LLUVIA-ESCURRIMIENTO; Coordinación de Investigación; Area de Riesgos Hidrometeorológicos; R. Domínguez, M. Jiménez, F. García y M.A. Salas

REPORT ON THE JANUARY 17, 1994 NORTHRIGDE EARTHQUAKE. SEISMOLOGICAL AND ENGINEERING ASPECTS; Coordinación de Investigación; Areas de Riesgos Geológicos y de Ensayes Sísmicos; T. Mikumo, C. Gutiérrez, K. Kikuchi, S. M. Alcocer y T. A. Sánchez.

APPLICATION OF FEM (FINITE ELEMENT METHOD) TO RC (REINFORCED CONCRETE) STRUCTURES; Coordinación de Investigación; Area de Ensayes Sísmicos, H. Noguchi.

DEVELOPMENT OF ADVANCED REINFORCED CONCRETE BUILDINGS USING HIGH-STRENGTH CONCRETE AND REINFORCEMENT -NEW CONSTRUCTION TECHNOLOGY IN JAPAN-; Coordinación de Investigación; Area de Ensayes Sísmicos; S. Otani.

A STUDY ON NONLINEAR FINITE ELEMENT ANALYSIS OF CONFINED MASONRY WALLS; Coordinación de Investigación; Area de Ensayes Sísmicos; K. Ishibashi; H. Kastumata; K. Naganuma; M. Ohkubo.

SEGURIDAD SISMICA DE LA VIVIENDA ECONOMICA; Coordinación de Investigación; Area de Ensayes Sísmicos; R. Meli; S.M. Alcocer; L.A. Díaz Infante; T.A. Sánchez; L.E. Flores; R. Vázquez del Mercado; R.R. Díaz.

DETERMINISTIC INVERSE APPROACHES FOR NEAR-SOURCE HIGH-FRECUENCY STRONG MOTION; Coordinación de Investigación; Area de Riesgos Geológicos; M. Iida.

SISMICIDAD Y MOVIMIENTOS FUERTES EN MEXICO: UNA VISION ACTUAL; Coordinación de Investigación; Area de Riesgos Geológicos; S. K. Singh, M. Ordaz.

JAPANESE PRESSS DESIGN GUIDELINES FOR REINFORCED CONCRETE BUILDINGS; Coordinación de Investigación; Area de Ensayes Sísmicos, S. Otani.

COMENTARIOS SOBRE LAS NORMAS INDUSTRIALES JAPONESAS DE LA CALIDAD DE AGREGADOS PARA EL CONCRETO; Coordinación de Investigación; Area de Ensayes Sísmicos; M. Saito, H. Kitajima, K. Suzuki, S. M. Alcocer.

COMENTARIOS SOBRE LAS NORMAS INDUSTRIALES JAPONESAS DE LA CALIDAD DEL CONCRETO; Coordinación de Investigación; Area de Ensayes Sísmicos, M. Saito, H. Kitajima, K. Suzuki, S. M. Alcocer.

NORMAS DE DISEÑO PARA ESTRUCTURAS DE MAMPOSTERIA DEL INSTITUTO DE ARQUITECTURA DEL JAPON; Coordinación de Investigación; Area de Ensayes Sísmicos; K. Yoshimura, K. Kikuchi, T. A. Sánchez.

RED DE OBSERVACION SISMICA DEL CENAPRED, REGISTROS ACELEROGRAFICOS OBTENIDOS DURANTE 1993, Coordinación de Investigación; Area de Instrumentación Sísmica; B. L.ópez, R.Quaas, S. Medina, E. Guevara, R. González.